JOURNAL OF PROPULSION AND POWER
Vol. 17, No. 1, January–February 2001

Mach 8 Testing of a Scramjet Engine Model

Takeshi Kanda,* Tetsuji Sunami,† Sadatake Tomioka,‡ Kouichiro Tani,‡ and Tohru Mitani§
National Aerospace Laboratory, Kakuda, Miyagi 981-1525, Japan

To improve combustion performance in a hydrogen-fueled scramjet research engine model for the Mach 8 flight condition, a thick strut was attached, and the contraction ratio was increased to 8.3. According to results obtained by gas sampling at the exit of the model, a combustion efficiency of 90% was attained for the fuel flow rate at $\phi = 0.8$. Normal fuel injection into the low-velocity region on the top wall where the recovery temperature was high was found to be effective for ignition. The high pressure in the combustor caused by the thick strut was also found to be effective for combustion. The thrust increase from the no-fuel condition was 420 N for $\phi = 1.2$. The relatively low thrust level was caused by the Rayleigh heating loss and the base drag of the strut. Small amounts of fuel injection upstream of the step changed the combustion condition significantly, however, controlled engine operation was difficult to achieve. Parallel fuel injection resulted in very poor combustion for this engine model.

Nomenclature

h	=	step height
P_w	=	wall pressure
P_1	=	nominal static pressure at the exit of the Mach 6.7 nozzle, pressure upstream of the shock train
P_2	=	increased pressure by combustion at the end of the shock train
x_c	=	combustion position in the one-dimensional calculation
$x1$	=	streamwise distance from the leading edge of the side wall
y	=	vertical distance from the top wall
z	=	spanwise distance from center plane
ΔF	=	thrust increase from no-fuel condition
η_c	=	combustion efficiency
ϕ	=	equivalence ratio of injected hydrogen fuel
ϕ_{local}	=	local equivalence ratio

Introduction

A STUDY of an aerospace plane is being carried out to create a new transportation system for travel to and from a low Earth orbit. A scramjet engine to be used in such an aerospace plane is being studied at the National Aerospace Laboratory (NAL), Kakuda Research Center. A subscale scramjet research engine model has been previously tested under Mach 4 and Mach 6 flight conditions in the Ramjet Engine Test Facility (RJTF).[1] Information from other subscale scramjet engine tests are not open, so the report on the tests at the RJTF is beneficial for the worldwide advance of the scramjet engine. Not only the data on the engine performance, but also many important features of the scramjet engine and the test facility were found from the tests. For example, the interaction between components affected the starting of the inlet.[2] Two combustion modes were observed; the mode with a high combustion efficiency was designated the intensive combustion mode.[3] Effects of the two air-heating methods, vitiation heating and storage heating, on combustion conditions were clarified.[4] Characteristics of the liquid-hydrogen cooling were also investigated.[5]

Received 1 June 1999; revision received 1 February 2000; accepted for publication 12 May 2000.

*Head, Ramjet Systems Section, Ramjet Propulsion Research Division, Kakuda Research Center. Senior Member AIAA.
†Researcher, Ramjet Propulsion Research Division, Kakuda Research Center. Member AIAA.
‡Senior Researcher, Ramjet Propulsion Research Division, Kakuda Research Center. Member AIAA.
§Head, Ramjet Combustion Section, Ramjet Propulsion Research Division, Kakuda Research Center. Member AIAA.

Under the Mach 8 flight condition, the subscale engine tests were also conducted. The Mach number and the enthalpy of the tests are the typical operating conditions of the scramjet engine. In the first series of the tests, the geometrical contraction ratio of the model was three, significantly lower than that of the design configuration, with the result that only slight thrust was produced.[6] In the second series, the engine followed the design configuration such that it had a strut, and the geometrical contraction ratio was five. That strut is designated as the standard strut here. The engine produced larger thrust, and autoignition was attained. However, a large amount of fuel ($\phi = 2.3$) was required to produce a thrust increase of 250 N from the no-fuel condition.[7]

In the present series, a thick strut was attached to the engine and the contraction ratio was increased to 8.3 to improve combustion performance. The modification was expected to decelerate the air, enhance the mixing, and increase the pressure. The tests showed a larger pressure increase by combustion, significant mixing, and high combustion efficiencies, but a low thrust increase from the no-fuel condition. In the present paper, the test condition and the principal test results are first presented briefly. Secondary discussions and analyses on the combustion condition and the thrust level follow. The results will be helpful for the design and modification of future scramjet engines and combined-cycle engines.

Experimental Apparatus and Methods

Test Facility

The RJTF is equipped with a high-temperature and high-pressure air supply system and a vacuum ejection system. The Mach number at the exit of the facility nozzle was 6.73. The total temperature and the total pressure of the air were 2600 K and 10.0 MPa, respectively. They correspond to flight conditions at Mach 8 with a flight dynamic pressure of 26 kPa. The relatively low dynamic pressure was due to the facility capacity. Compressed air was heated by a ceramic storage heater and subsequently heated by a vitiation air heater. At the nominal operation, the flow rates of air, hydrogen, and oxygen for the vitiation heater were 6.16, 0.181, and 2.16 kg $\cdot$ s^{-1}, respectively. The vitiated air contained 21% oxygen and 27% water in volume fraction. The supersonic facility nozzle had exit dimensions of 51 $\times$ 51 cm. The nominal static pressure at the exit of the nozzle was 1.6 kPa. The boundary-layer thickness was 90 mm at the engine entrance, according to pitot pressure measurements.[8] The inner surface of the top wall of the engine model coincided with that of the Mach 6.73 nozzle to ingest the boundary layer, simulating the entrance conditions of the engine of the aerospace plane.

Engine Model

Figure 1 shows a schematic diagram of the water-cooled engine model. The top wall was at $y = 0$ mm and the cowl inner surface

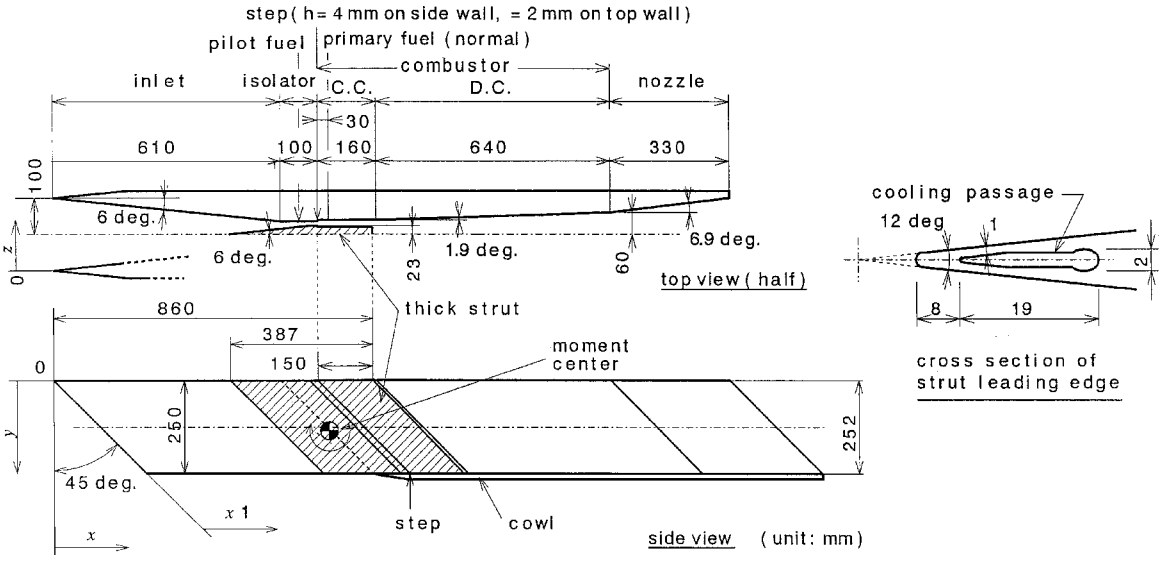

Fig. 1 Schematic of the water-cooled scramjet engine model with a strut.

was at $y = 250$ mm. The swept angle of the side wall and the strut was 45 deg. The half wedge angle of 6 deg of the thick strut was the same as that of the standard strut used in the second series of the Mach 8 tests[7] and in Mach 6 tests.[9] The new, thick strut had to be located on the top wall between the inlet and the constant duct part of the combustor (CC), and the strut had a wide base area due to the attachment restriction. The strut was expected to improve combustion, but was not expected to increase the thrust significantly due to an anticipated large base drag.

The parallel part of the side wall commenced at $x1 = 609.8$ mm. The geometrical contraction ratio including the strut was 5.00 and the ratio without the strut was 2.86 at $x1 = 609.8$ mm. The projected cross section at the entrance of the engine, that is, 200×250 mm, was used as a reference area here. The leading edge of the cowl was also located at $x1 = 609.8$ mm. The parallel part of the thick strut commenced at $x1 = 685.9$ mm. The gap between the side wall and the strut was 12 mm, and the geometrical contraction ratio took a maximum value of 8.33 here. There was a backward-facing step at the junction of the isolator (Is) and the combustor for isolation of the pressure increase in the combustor and for flame holding. Its height was 4 mm on the side walls and on the strut and 2 mm on the top wall. The location of the step of the thick strut was the same as that of the side walls, that is, $x1 = 709.8$ mm. The gap was 20 mm between the side wall and the strut, and the geometrical contraction ratio decreased to 8.27 downstream of the steps. No fuel was injected from the strut. The strut base was located 10 mm upstream of the end of the parallel part of the side wall. The geometrical contraction ratio was 2.54 just downstream of the strut base. The divergent angle of the side wall changed at $x1 = 1510$ mm. There, the gap between the side walls was 120 mm. The geometrical contraction ratio of 0.99 at the exit of the engine was slightly smaller than unity due to the step on the top wall in the combustor.

The hydrogen fuel was injected at sonic speed normal to the side walls through 24 holes located 30 mm downstream of the step, or parallel to the side walls through 24 holes on the side-wall steps at the Mach number of 2.9. The throat diameters of the normal injectors and the parallel injectors were 1.5 mm, and the exit diameter of the parallel injectors was 3.0 mm. The total temperature of the fuel was approximately 280 K, and the total pressure of the fuel varied up to 3.5 MPa, according to the fuel flow rate. Supplementary fuel for flame holding at the step, which is designated as the pilot fuel here, was supplied with sonic speed through 94 holes on the side walls 50 mm upstream of the step, the diameter of each being 0.5 mm. Fuel flow rates were measured by metering orifices. The model had no igniter because autoignition was confirmed in the previous Mach 8 tests.[7] The fuel flow rate at the stoichiometric condition was $47\ \mathrm{g \cdot s^{-1}}$. It was calculated with the assumption that the mass capture ratio was 0.85 from a computational fluid dynamics (CFD) simulation of the present tests.[10] The fuel condition in each test is represented by the test number and a letter, for example, 17a, 17e, etc.

The normal fuel injectors were designed based on the experimental results of the supplementary tests at NAL.[11] In the tests, the normally injected fuel jets interacted with the boundary layer behind the backward-facing step, and a large separation region was created between the jets and the step. The interaction caused higher combustion efficiency and a larger penetration of fuel, also shown in the tests at the RJTF.[3] In the design procedure for the engine used at the RJTF, the mechanism for this was not sufficiently clear. Thus, because of the long distance between the step and the injectors, the interaction was hard to achieve, and the penetration of the fuel was limited in the flow.

The engine wall was made of copper. The engine components individually cooled by water were 1) the leading edge of the inlet, 2) the inlet, 3) the top walls of the isolator and the CC, 4) the side walls of the isolator and the CC, 5) the cowl, 6) the divergent duct part of the combustor (DC), 7) the nozzle, and 8) the leading edge of the strut. The cooling channel of the leading edge of the strut is shown in Fig. 1. Because only the leading edge was cooled in the strut, the test duration time was limited to 15 s.

Measurements

Wall Pressure and Heat Flux

In the present paper, the wall pressure is nondimensionalized with the nominal static pressure at the exit of the Mach 6.73 nozzle. In the figures discussed hereafter, the pressure on the top wall was measured along the centerline of the channel. The pressure distributions on the side wall are also shown at three positions;

1) The first position is the vicinity of the top wall, that is, $y = 10$ mm in the inlet and at $y = 45$ mm downstream of the inlet. This position is designated as side wall near the top wall in the figures.

2) The second position is $y = 125$ mm. This position is designated as side wall at the midheight.

3) The third position is the vicinity of the cowl, that is, $y = 240$ mm from the inlet to the end of the CC and at $y = 210$ mm in the DC and the nozzle. This position is designated as side wall near the cowl.

The wall pressure positions are not arranged at the specified y coordinates because of the arrangement of the cooling water passages. The measurement error of the nondimensionalized wall pressure was ± 0.3 in the inlet, ± 0.06 in the isolator and CC, and ± 1 in the DC and nozzle.

Heat flux was estimated from the rate of the temperature change of the cooling water and the water flow rate. The error associated with heat fluxes was ±0.15 MW.

Force and Momentum

Thrust was measured by a floating frame force measurement system (FMS). The error of the measured forces was ±50 N. The measured thrust/drag by the FMS contained additional drag that should not be included in the net thrust estimation. Therefore, only the increase of the thrust caused by the combustion from that in the no-fuel condition is evaluated and is shown in the figures and listed in tables.

Gas Sampling and Pitot Pressure Measurement

Gas sampling and pitot pressure measurement were carried out at 60 locations at the exit of the engine model using probes, each with a sampling orifice of 0.3 mm, after probe calibration.[12] With the measured results by the gas sampling and the pitot pressure measurement, the distributions of equivalence ratio, mass flux, and the combustion efficiency were obtained. The combustion efficiency was calculated from the change of the oxygen/nitrogen ratio of the sampled gas to the ratio of the wind-tunnel vitiated air, taking account of the equivalence ratio. The error of the combustion efficiency was ±5%, including the error of measuring systems and the quenching effect in the sampling probe. The error of the equivalence ratio measure and that of the pitot pressure were ±3% each.

One-Dimensional Calculation

A one-dimensional calculation was conducted to estimate the flow condition in the engine model. The model was used in the previous investigation on the test results at the RJTF.[3] Assumptions and calculation conditions were as follows:

1) The effect of the swept angle was ignored and the distance from the leading edge was used when the calculated results were compared with the experimental data.

2) The air and the combustion gas were equilibrium flows through the engine.

3) The inlet kinetic energy efficiency was taken as 0.99 from the pressure distribution in the inlet of the present model. The mass capture ratio was 0.85 according to the estimation by CFD.

4) The specified part of hydrogen burned quickly in a stoichiometric condition at the specified location. The combustion efficiency in this one-dimensional model was defined as the ratio of the specified burned to the injected hydrogen. The residual hydrogen was mixed with the residual air.

5) The combustion gas and the noncombusted mixture expanded isentropically in the DC.

6) The boundary layer was turbulent throughout the engine. The friction coefficient was calculated with the formula of van Driest (see Ref. 13).

Experimental Results

Combustion with Normal Fuel Injection

In this section, principal results are presented. First, a chart of the thrust vs the fuel flow rate is shown to illustrate the test results. Then details of the engine operating conditions are presented, including distributions of the wall pressure, local combustion efficiencies, and other results. In the present tests, a high combustion efficiency was measured with normal fuel injection, but the associated thrust increase was small.

Thrust Increase

Figure 2 shows the thrust increase due to combustion measured from the no-fuel condition. When normal fuel injection was employed, the thrust increase was approximately proportional to the fuel flow rate. When the fuel equivalence ratio was larger than 1.2, the engine operated in the unstarted condition. Between $\phi = 0.8$ and 1.2, hysteresis was observed between the started and the unstarted conditions. In this region, when the fuel flow rate decreased in the unstarted condition during a test, the engine remained in the unstarted condition.

Table 1 Thrust by normal fuel injection

Test no.	Fuel flow rate, g · s^{-1} Normal	Parallel	Side-wall pilot	Equivalence ratio	Thrust increase from no-fuel condition, N
17e	38.7	0	0	0.82	253
16d	9.2	0	0	0.20	27
21b	56.1	0	0	1.19	421
15d	41.9	0	0	0.89	−10 (unstarted)
27c	60.4	0	0	1.29	2 (unstarted)

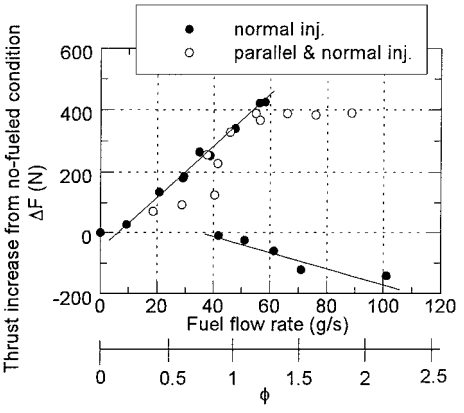

Fig. 2 Thrust increase from that in the no-fuel condition.

When the parallel fuel injection was combined with the normal fuel injection, the region of the started condition was enlarged, but the thrust level was lower than the thrust with normal injection. The scatter of the thrust data was due to the various combinations of the injected fuel flow rates.

A drag of 780 N in the no-fuel condition was measured by FMS. The force measured by FMS includes additional drag besides the net drag. Here, the net drag is defined as a sum of the drag on the inside of the engine and on the outer surface of the cowl, whereas the additional drag is a sum of the drag on the outer surface of the side walls and on the force measuring stand. According to the force measurement in the supplementary tests,[14] the net drag in the no-fuel condition was estimated to be 320 N. In the condition of $\phi = 1.2$ by the normal fuel injection at 21b, the net thrust was estimated to be 100 N.

Wall Pressure Distribution

Figures 3a–3d show the wall pressure distributions with normal fuel injection at four lateral locations. The associated fuel flow rates and the thrusts are listed in Table 1. The initial lower pressure on the top wall in comparison to the side wall was caused by the airflow being turned toward the cowl by the shock wave reflections in the convergent component with the swept angle. When the fuel flow rate was increased, the wall pressure as well as the thrust increased.

With fuel injection, the top wall pressure increased significantly in the isolator, that is, upstream of the step and the fuel injectors (Fig. 3a). On the side wall near the top wall and at the midheight, the wall pressure increased downstream of the fuel injector position, and the increase became notable from $x1 = 1000$ mm in the DC (Figs. 3b and 3c). On the side wall near the cowl, the pressure around the injectors reached that predicted using simple models for combustion at half-atmosphere pressure[15] (Fig. 3d). However, there was only a small increase of the wall pressure from that found in the no-fuel condition. These distributions were different from those of the intensive-combustion mode in the Mach 6 tests, in which the wall pressure significantly increased near the cowl on the side walls and also increased behind the step.[3]

The simulation result at $\phi = 0.8$ with the one-dimensional flow calculation is shown in Fig. 4. In the calculation, the fuel was injected normally in the CC and burned at $x1 = 1000$ mm in the DC instantaneously. This combustion position was determined from the

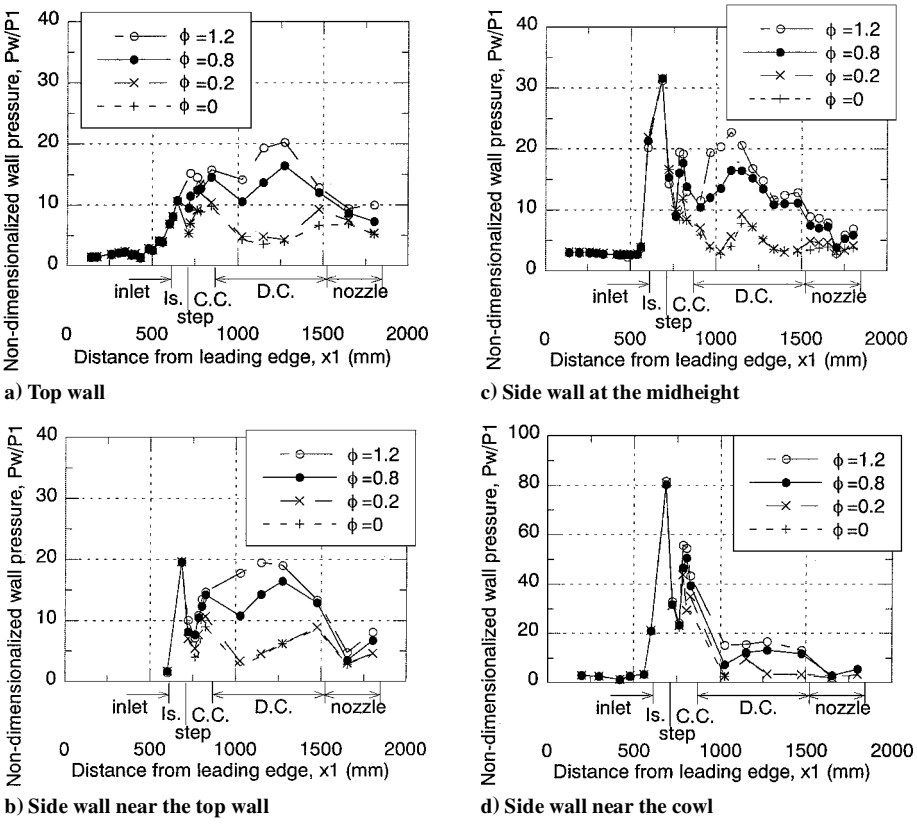

Fig. 3 Wall pressure distributions with normal fuel injection.

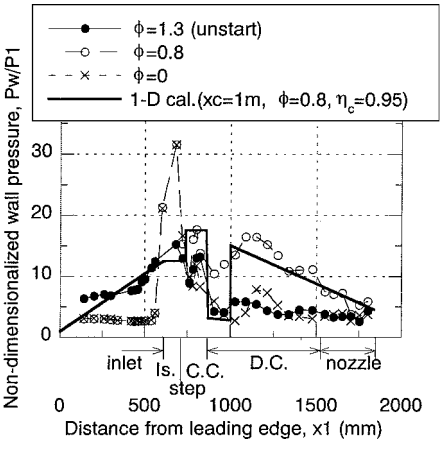

Fig. 4 Simulated wall pressure distribution by the one-dimensional calculation and the wall pressure distributions in the unstarted condition with normal fuel injection on the side wall at the midheight.

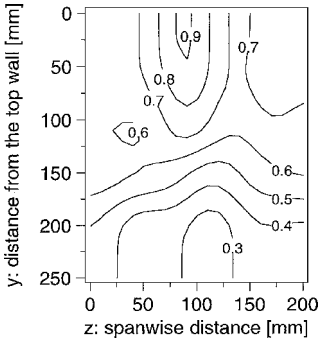

Fig. 5 Distribution of local equivalence ratio at the engine exit with fuel flow rate ϕ = 0.8 by normal injection.

experimental results. The combustion efficiency was assumed to be 0.95 in the calculation. The calculated pressure distribution shows reasonably good agreement with the experiment. The combustion efficiency at $\phi = 0.8$ was estimated to be about 0.9 in the experiment using one-dimensional calculations.

When the engine model was in the unstarted condition, the wall pressure in the inlet was higher than that in the airflow condition (Fig. 4). The side wall pressure was as high as that of the no-fuel condition downstream of the step.

Mixing and Combustion Efficiency

The thrust increased with the normal fuel injection, and the engine stayed in the started condition below $\phi = 0.8$. Therefore, gas sampling was conducted for normal fuel injection with $\phi = 0.8$. Figure 5 illustrates the distribution of the local equivalence ratio of hydrogen measured at the exit of the engine on a swept-back plane. Hydrogen was concentrated in the center region around $z = 100$ mm, near the top wall. The distribution of the equivalence ratio shows a different feature from that in the Mach 6 tests. In the intensive-combustion mode of the Mach 6 tests, rich hydrogen regions were formed in the corners between the top wall and the side walls.[9] On the whole, however, hydrogen spread well in the spanwise direction. In the vertical direction, hydrogen was concentrated on and near the top wall, similar to that observed in the Mach 6 tests.[4]

The contour lines of local combustion efficiency for the tests just described are shown in Fig. 6. A narrow region with combustion efficiency lower than 85% was found at the center of the top wall. However, in most regions, the combustion efficiencies were higher than 85% with the average being about 90%. A general tendency for the lower combustion efficiency to be located in the richer region was noted in the present testing.

Heat Flux

The heat flux experienced by the isolator and the CC was 2 $MW \cdot m^{-2}$ in both the no-fuel condition and the combustion condition. This indicates that the fuel did not burn in the CC significantly. The heat flux in the DC was about 0.8 $MW \cdot m^{-2}$ with $\phi = 0.8$, whereas it was about 0.3 $MW \cdot m^{-2}$ in the no-fuel condition. The change was larger than the error ± 0.15 MW. This indicates that

Table 2 Effects of parallel fuel injection and pilot fuel injection

Test no.	Fuel flow rate, g · s^{-1} Normal	Parallel	Side-wall pilot	Equivalence ratio	Thrust increase from no-fuel condition, N
26e	0	40.4	0	0.86	124
26f	48.1	40.4	0	1.88	389
20c	38.7	0	11.3	1.06	−73 (unstarted)
28f	0	28.4	3.8	0.69	202

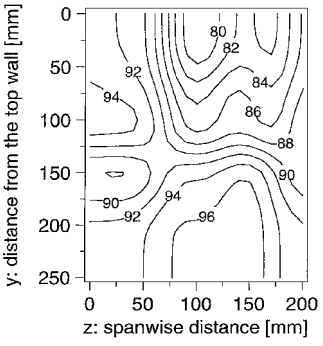

Fig. 6 Contour lines of local combustion efficiency at the engine exit with fuel flow rate ϕ = 0.8 by normal injection.

the combustion occurred primarily in the DC. In the unstarted condition, the heat flux in the inlet slightly increased from 0.2 MW · m^{-2} for the started condition to 0.4 MW · m^{-2} and decreased in the DC to 0.4 MW · m^{-2}. This feature was similar to that seen in the Mach 6 tests.[3]

Combustion with Other Fuel Injection Methods

When the fuel was injected from the parallel fuel injectors, little thrust was produced as shown in Table 2 for the case 26e. The slight increase of thrust was mainly caused by the jet thrust associated with the fuel injection nozzles. The thrust by the tangentially injected fuel jet was estimated to be 90 N at the fuel flow rate of 40 g · s^{-1}, and it was 70% of the measured thrust increase at 26e. When large amounts of fuel were supplied from both the normal fuel injectors and the parallel fuel injectors, the engine remained in the started condition, as seen in 26f and in Fig. 2.

When the pilot fuel injection upstream of the step was used with the normal injection downstream of the step, the unstarted condition occurred in 20c (Table 2). When the larger amount of fuel was supplied from the normal fuel injectors alone, the engine was in the started condition in 21b as shown in Table 1. When a small amount of fuel was injected from the pilot fuel injectors with the parallel fuel injection, the engine produced higher thrust (28f). Use of the pilot fuel injection increased thrust. However, control of the combustion condition by use of the pilot fuel injection was difficult in the present testing, because the mechanism of the combustion enhancement was not clear and the results were highly sensitive to the pilot flow rate.

According to Ref. 16, when there was the secondary injection upstream of the primary injection, the boundary layer was disturbed and the penetration height of the primary jet increased. This disturbance mechanism might have improved the combustion condition in the present tests. The blowing parameter was 10 with the injection of the pilot fuel at 8 g · s^{-1}, that is, $\phi = 0.17$. In the Mach 6 tests, intensive combustion was attained by the addition of the pilot fuel injection of 8.4 g · s^{-1} ($\phi = 0.06$) to the normal injection of 36 g · s^{-1} ($\phi = 0.25$) (Ref. 3). The blowing parameter was also 10 in this test.

Discussion

First, discussions on the combustion mode and the effect of the air heating mode on the engine performance are presented to clarify the engine operating condition for the present tests. Second, the reasons and the mechanisms underlying the test results including the characteristic distribution of the hydrogen fuel, the high combustion efficiency and the low thrust level are discussed.

Mixing-Controlled Combustion in Mach 8 Tests

In unsteady flow consisting of turbulent eddies, lean and rich mixtures are collected alternately by a gas-sampling probe. These mixtures contain excess oxygen or hydrogen even if the deficient reactant is completely consumed, that is, if the instantaneous combustion efficiency is unity. They are eventually mixed in the sampling bottle and indicate a lower time-averaged combustion efficiency. This effect becomes pronounced in near-stoichiometric mixtures. If the combustion is rate-controlled by chemical reaction rates, the combustion efficiency should not decrease at the stoichiometric condition. Regarding the present experimental results as shown in Figs. 5 and 6, a low combustion efficiency of around 80% was observed for a near-stoichiometric condition of $\phi_{local} = 0.9$. This indicates that the engine model operated in the mixing-controlled regime in the Mach 8 flight condition tests. It implies that dependence of the engine performance on air heating modes[4] may not have been strong in the tests.

Distribution of Hydrogen Fuel

In the vertical direction, hydrogen was concentrated on and near the top wall. One of the reasons for this distribution of hydrogen in the vertical direction was the nonuniformity of the mass flux of the air entering the combustor. According to measurement, the flux of the air was about 1.5 times larger near the cowl than near the top wall, resulting in small concentrations of hydrogen near the cowl. The air turned toward the cowl in the inlet and the isolator, and the flux was large around the cowl. Another reason for this was the flow deflection toward the top wall through expansion fans from the ridges with a swept-back angle, especially the fan from the rear corner of the strut. The velocity component vertical to the ridge increases through the expansion fan, whereas the tangential component to the ridge is conserved. The mechanism of the flow direction change resembles that in the inlet with a swept-back angle. The injected hydrogen was probably carried by the deflected airflow in the DC.

The local equivalence ratios show relatively uniform distribution in the spanwise direction, even far from the fuel injectors. The penetration height of the normally injected fuel was small as described earlier and was estimated to be 3 mm by the formula of Ref. 16 at the condition of fuel flow rate at $\phi = 0.8$, the total pressure of the fuel at 2.1 MPa, and the ratio of the dynamic pressure of the fuel to that of the airflow at 3.5. The gap between the strut and the side wall was 20 mm, much larger than the penetration length. Therefore, the concentration toward the center in the spanwise direction was not caused by the increase of the penetration of the fuel.

One of the possible mechanisms for the observed hydrogen spread is turning of the flows through the expansion fan from the strut. The airflow spreads to the center through the expansion fan from the rear corner of the strut. The normally injected hydrogen fuel is turned and conveyed by the airflow, resulting in the observed spread of the hydrogen. If the fuel is accelerated to the velocity of the airflow after injection, the Mach number of the hydrogen fuel is estimated to be 2.5, which is lower than 5 of the airflow in the combustor. Here, the nominal velocity of airflow in the engine is 2000 m · s^{-1}, which was estimated from the wall pressure. The airflow turned approximately 20 deg and the pressure decreased through the expansion fan.[17] If the fuel had expanded to the decreased pressure, the turning angle of the hydrogen fuel would have been about 30 deg. This indicates intensive interaction between the fuel and the air and that the interaction promoted mixing.

A slight concentration of the hydrogen downstream of the strut was observed in the Mach 6 tests.[9] In the Mach 6 tests, the difference of the Mach numbers between the fuel hydrogen and the airflow was small, and the interaction must have been weak. In the Mach 6 tests with the short strut, which was attached on the top wall with height one-fifth that of the engine height, the region with the aforementioned interaction was restricted, and mixing was not promoted.

Ignition and Combustion in Mach 8 Flow Condition

On the top wall, there existed a thick boundary layer with a height of about 40% of the engine. The airflow was decelerated through

the many shock wave reflections in the inlet and the isolator and the low-velocity region on the top wall was thickened. In addition, the airflow in the convergent section with the swept angle was turned toward the cowl, and this turning thickened the low-velocity region on the top wall. Such thickening was observed in the Mach 4 test condition.[18] The height of the subsonic region on the top wall was estimated to be about 30 mm from the CFD result.[10]

As described in the preceding section, the engine operated in the mixing-controlled combustion regime in the Mach 8 test condition, that is, chemical reactions progressed relatively fast. The ignition time at a static pressure of 15 kPa and a total temperature of 2600 K was estimated to be 2×10^{-5} s for the thick-strut model.[19] Here, the ignition time was defined as the time required to raise the total temperature 5% by combustion. The ignition distance was, thus, 40 mm for a flow velocity of 2000 $m \cdot s^{-1}$, which is the nominal velocity of airflow in the engine. Temperatures as high as the recovery temperature were required for ignition. Sufficiently high temperature was attained in the low-velocity region on the top wall. The first normal fuel injection port was at $y = 5$ mm from the top wall. From it, the fuel was injected into the low-velocity region. Because the top wall pressure began to increase in the isolator, ignition and subsequent combustion are believed to have initiated in the low-velocity region around the step and the fuel injectors. Such low-velocity regions did not exist other than on the top wall in the present engine. In the Mach 6 tests with the intensive combustion mode, the low-velocity region also existed around the cowl surface. This difference in position of the low-velocity region clarifies the difference in the combustion conditions between the Mach 6 and the Mach 8 tests.

The combustion time scale and the combustion length were estimated to be 5×10^{-4} s and 1 m in the CC in the thick-strut model and 3×10^{-3} s and 6 m in the no-strut model. Here, the combustion time scale is defined as the time required to raise the temperature from 5 to 95% of the equilibrium temperature rise. The combustion length is the product of the combustion time and the nominal velocity of airflow in the CC of 2000 $m \cdot s^{-1}$. The combustion process is strongly affected by pressure. Though the pressure level was much lower than that in the isolator, the pressure level in the DC was higher in the thick-strut model than in the no-strut model or the standard-strut model with the contraction ratio of five. This pressure level worked well to shorten the combustion time scale.

The preceding combustion lengths were estimated for the fully mixed case. The combustion actually completed further downstream than at the estimated length due to fuel–air mixing. However, in the experiments, the combustion process seemed to be completed rapidly, even though in basic two-dimensional turbulent mixing layers, mixing is slow.[15] In the thick-strut model, around the top wall, the mixing progressed rapidly in the low-velocity region. The mechanism of hydrogen spread through the expansion fan and the deflections to and from the top wall also promoted mixing of the hydrogen with the air and, thus, shortened the combustion time. The reacted gas would be also carried by the spreading mechanism of the hydrogen. The carried combustion gas induced the subsequent reaction far from the low-velocity region on the top wall.

The base region of the strut was also the low-velocity region in the combustor. However, the region did not directly contribute to enhanced combustion in the present tests. The measured pressure for the strut base at $y = 125$ mm did not change during a test in the started condition. As mentioned before, the penetration of the fuel jet injected from the side walls was small, and the fuel jet did not reach the base other than on the top wall. In addition, base pressure is significantly low and it is not favorable to burning.

The first parallel-injection port was in the low-velocity region at $y = 15$ mm from the top wall. The injectant had a velocity of approximately 2000 $m \cdot s^{-1}$ at the parallel fuel injector exit such that not much of it remained in the low-velocity region. The velocity was similar to that of the airflow, and any mixing of the airflow with the fuel was limited.

Reason for the Low Thrust

In the present tests, a high combustion efficiency was achieved, but the thrust increase was small. The specific impulse was 2000 $m \cdot s^{-1}$ with the estimated net thrust of 100 N at $\phi = 1.2$. One reason for the small achieved thrust was the large base drag of the strut. An increase in pressure was observed far downstream of the strut except on the top wall. The pressure on the base plane of the strut was low, and the resultant drag of the overall strut was large. Another reason for the small thrust was the Rayleigh heating loss due to combustion in the expanded, high-Mach-number flow. The increased pressure caused by the addition of heat decreases with the increase of the Mach number of the flow. Because the possible region of ignition was only on the top wall in the present engine, the radicals would be carried from that region to downstream in the engine, and the combustion would succeed in the DC, where the Mach number was rather high. Thus, the heating loss became large in this engine.

The thrust of the engine model can possibly be increased by modification of the strut base shape and by moving the combustion position upstream. According to the one-dimensional calculation, when there is combustion at the injector position with a combustion efficiency of 95% at $\phi = 0.8$, the calculated net thrust will be 800 N and the specific impulse will be 16000 $m \cdot s^{-1}$. To attain such operation, the creation of the low-velocity region on the side walls is necessary for short ignition time and enhanced mixing. Avoiding the unstarted condition discussed hereafter is also necessary.

Unstarted Condition

The combustion in the CC near the injectors will be necessary for decreasing the heating loss and increasing the thrust. However, it was pointed out that the combustion in the CC would cause the unstarted condition in the engine with the standard strut.[7] In the present engine, with the thick strut, the Mach number in the isolator was about four according to the one-dimensional calculation and the measured wall pressure. The separation pressure[20] in the isolator was about 130 kPa. When there is combustion in the CC, the increased pressure due to the combustion at the combustion efficiency of 0.95 will be 150 kPa at $\phi = 1.0$, according to the one-dimensional calculation. The pressure due to the combustion is higher than the separation pressure. Therefore, there will be a shock train in the isolator. The shock train is anticipated to become long on the top wall, where the low-velocity region is.

The shock train length in the duct was estimated by an empirical formula,[21] in which momentum thickness is required. A momentum thickness of 40 mm at the entrance of the engine was used here. The thickness was 15 mm in the Mach 4 test condition and 30 mm in the Mach 6 test condition. In the estimation by the formula, the duct height was replaced by the gap of the flow channel in the engine. Measured pressures on the top wall at the entrance of the isolator P_1 were used for the upstream values of the shock trains, and estimated results are shown in Fig. 7 with origin at the step. The increased pressure by combustion P_2 was assigned at the step. The shock train length is the length between the position of P_2 and the initial position of the shock train. The experimental results are also shown in Fig. 7. Measured maximum top wall pressures within the started condition are plotted as P_2 against the length of the isolator. Here, the started condition is defined such that combustion does not affect the pressure distribution in the inlet. In the limit of the started condition, the shock train would start at the entrance of the isolator, and the length of the shock train in the experiments was almost the same as that of the isolator. In some tests, a long isolator (LI) was used. Its length was 200 mm, longer than that of the short isolator (SI) of the present model whose length was 100 mm. In the Mach 4 tests, there was no strut. In the Mach 6 tests, two kinds of struts were used, the one-fifth strut whose height was one-fifth of the engine height[3] and the standard strut.[9]

In the Mach 4 test conditions, the model fell into the unstarted condition due to the development of the separation on the top wall.[2] The estimated results agreed with the experimental observations. In the Mach 6 tests, the unstarted condition initiated with a lower pressure increase than in the calculation. It was caused by the fact that the engine fell into the unstarted condition due to the separation on the cowl in the Mach 6 tests.[3]

In the present Mach 8 tests, when there is combustion with $\phi = 1.0$ and combustion efficiency of 95% in the CC, the average pressure

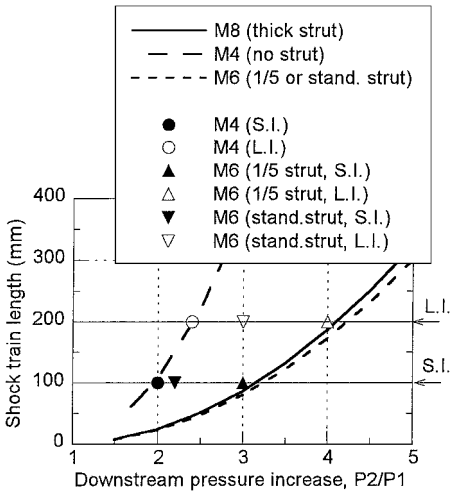

Fig. 7 Estimated shock train lengths in the isolator for Mach 4, 6, and 8 test conditions.

is estimated to be 150 kPa. Because the experimental top wall pressure in the airflow condition was low around 15 kPa at the step position, the ratio of the pressure increase will be large up to 10. According to the estimation results of the shock train, an isolator of approximately 1 m will be necessary to contain the pressure increase. The thick strut thickened the low-velocity region on the top wall, and the region was favorable to ignition. However, the thick low-velocity region increased the upstream-influence distance and the length of the shock train. The low-pressure level on the top wall was also a negative factor for the started condition. To shorten the shock train, the low-velocity region should be thinned, or the ratio of the pressure increase should be decreased on the top wall in the isolator.

Concluding Remarks

To improve combustion conditions, a scramjet engine model with a thick strut was tested under the Mach 8 flight condition of the RJTF. The engine geometrical contraction ratio was 8.3. The following points were clarified from the tests and the discussions.

1) The hydrogen fuel burned well in the thick-strut engine model with a combustion efficiency of 90% at the flow rate of $\phi = 0.8$.

2) The ignition condition was easily attained in the hot, low-velocity region on the top wall in the combustor. The region was due to the thick boundary layer and the turning of the airflow toward the cowl. High pressure in the combustor by the thick strut was found to be effective for combustion.

3) The unstarted condition was caused by the thick, low-velocity region and the low-pressure level on the top wall.

4) The thrust increase from the no-fuel condition was 420 N at $\phi = 1.2$. The small thrust was due to the Rayleigh heating loss and the base drag of the strut. The large heating loss was due to the fact that the ignition region was limited to the top wall in the engine.

5) With parallel fuel injection, fuel did not react significantly. However, pilot fuel injection upstream of the step changed the combustion conditions.

Acknowledgments

The present study was conducted as a part of the program of NAL–Mitsubishi Heavy Industries Ltd. cooperative research. The authors wish to thank the members of the scramjet research group of NAL for cooperation in testing, data processing, and discussion.

References

[1]Yatsuyanagi, N., Chinzei, N., Mitani, T., Wakamatsu, Y., Masuya, G., Iwagami, S., Endo, M., and Hanus, G., "Ramjet Engine Test Facility (RJTF) in NAL-KRC, Japan," AIAA Paper 98-1511, April 1998.

[2]Sunami, T., Sakuranaka, N., Tani, K., Hiraiwa, T., and Shimura, T., "Mach 4 Tests of a Scramjet Engine—Effect of Isolator," *Proceedings of 13th International Symposium on Air Breathing Engines*, AIAA, Washington, DC, 1997, pp. 615–625.

[3]Kanda, T., Hiraiwa, T., Mitani, T., Tomioka, S., and Chinzei, N., "Mach 6 Testing of a Scramjet Engine Model," *Journal of Propulsion and Power*, Vol. 13, No. 4, 1997, pp. 543–551.

[4]Mitani, T., Hiraiwa, T., Sato, S., Tomioka, S., Kanda, T., and Tani, K., "Comparison of Scramjet Engine Performance in Mach 6 Vitiated and Storage-Heated Air," *Journal of Propulsion and Power*, Vol. 13, No. 5, 1997, pp. 635–642.

[5]Wakamatsu, Y., Chinzei, N., Ono, F., Saito, T., Kanda, T., Tomioka, S., and Yatsuyanagi, N., "Design and Preliminary Experiments of Liquid Hydrogen Cooled Scramjet Engine," *Proceedings of the 21st International Symposium on Space Technology and Science (ISTS)*, ISTS Committee, Paper 98-a-1-27, Tokyo, May 1998.

[6]Saito, T., Wakamatsu, Y., Mitani, T., Chinzei, N., Shimura, T., and Kanda, T., "Mach 8 Testing of a Scramjet Engine Model," *Proceedings of the 20th International Symposium on Space Technology and Science*, Vol. 1, International Symposium on Space Technology and Science Committee, Tokyo, 1996, pp. 58–63.

[7]Tomioka, S., Kanda, T., Tani, K., Mitani, T., Shimura, T., and Chinzei, N., "Testing of a Scramjet Engine with a Strut at Mach 8 Flight Condition," AIAA Paper 98-3134, July 1998.

[8]Hiraiwa, T., Mitani, T., Izumikawa, M., and Ono, F., "Calibration Studies of Nozzle Flow in Ramjet Engine Test Facility," *Proceedings of the 20th International Symposium on Space Technology and Science (ISTS)*, ISTS Committee, Paper 96-d-14, Tokyo, May 1996.

[9]Sato, S., Izumikawa, M., Tomioka, S., and Mitani, T., "Scramjet Engine Test at Mach 6 Flight Condition," AIAA Paper 97-3021, July 1997.

[10]Kodera, M., Sunami, T., and Nakahashi, K., "Numerical Analysis of Scramjet Combusting Flows by Unstructured Grid Method," AIAA Paper 2000-0886, Jan. 2000.

[11]Chinzei, N., Komuro, T., Kudou, K., Murakami, A., Tani, K., Masuya, G., and Wakamatsu, Y., "Effects of Injector Geometry on Scramjet Combustor Performance," *Journal of Propulsion and Power*, Vol. 9, No. 1, 1993, pp. 146–152.

[12]Mitani, T., Takahashi, M., Tomioka, S., Hiraiwa, T., and Tani, K., "Analyses and Application of Gas Sampling to Scramjet Engine Testing," *Journal of Propulsion and Power*, Vol. 15, No. 4, 1999, pp. 572–577.

[13]White, F. M., *Viscous Fluid Flow*, McGraw–Hill, New York, 1974, pp. 632–640.

[14]Mitani, T., Kanda, T., Hiraiwa, T., Igarashi, Y., and Nakahashi, K., "Drag in Scramjet Engine Testing: Experimental and Computational Fluid Dynamic Studies," *Journal of Propulsion and Power*, Vol. 15, No. 4, 1999, pp. 578–583.

[15]Heiser, W. H., Pratt, D. T., Daley, D. H., and Mehta, U. B., *Hypersonic Airbreathing Propulsion*, edited by J. S. Przemieniecki, AIAA Education Series, AIAA, Washington, DC, 1994, pp. 233, 280–313.

[16]Cohen, L. S., Coulter, L. J., and Egan, W. J., Jr., "Penetration and Mixing of Multiple Gas Jets Subjected to a Cross Flow," *AIAA Journal*, Vol. 9, No. 4, 1971, pp. 718–724.

[17]Chang, P. K., *Separation of Flow*, 1st ed., Pergamon, Oxford, England, U.K., 1970, pp. 531–607.

[18]Kodera, M., Nakahashi, K., Hiraiwa, T., Kanda, T., and Mitani, T., "Scramjet Inlet Flow Computations by Hybrid Grid Method," AIAA Paper 98-0962, Jan. 1998.

[19]Mitani, T., Chinzei, N., and Kanda, T., "Reaction- and Mixing-Controlled Combustion in Scramjet Engines," AIAA Paper 99-4871, Nov. 1999.

[20]Zukoski, E. E., "Turbulent Boundary-Layer Separation in Front of a Forward-Facing Step," *AIAA Journal*, Vol. 5, No. 10, 1967, pp. 1746–1753.

[21]Sullins, G., and McLafferty, G., "Experimental Results of Shock Trains in Rectangular Ducts," AIAA Paper 92-5103, Dec. 1992.